OPEN ACCESS

Japanese Journal of Applied Physics **65**, 038003 (2026) **BRIEF NOTE**

https://doi.org/**10.35848/1347-4065/ae42ac**

Mapping primary crystallographic planes in β-Ga_2O_3 based on a pseudo-cubic oxygen sublattice

Takayoshi Oshima*

Research Center for Electronic and Optical Materials, National Institute for Materials Science, Tsukuba, Ibaraki 305-0044, Japan

*E-mail: OSHIMA.Takayoshi@nims.go.jp

Received January 18, 2026; revised February 3, 2026; accepted February 4, 2026; published online February 16, 2026

Although β-Ga_2O_3 crystallizes in the monoclinic system, its structural complexity can be simplified by focusing on the oxygen framework. The oxygen sublattice forms a cubic close-packed arrangement, corresponding to a distorted face-centered cubic (fcc) structure defined by lattice vectors: $\boldsymbol{a}_{\mathbf{fcc}} = \boldsymbol{b} + 1/2\ \boldsymbol{c}$, $\boldsymbol{b}_{\mathbf{fcc}} = -\boldsymbol{b} + 1/2\ \boldsymbol{c}$, $\boldsymbol{c}_{\mathbf{fcc}} = 1/3\ \boldsymbol{a} + 1/6\ \boldsymbol{c}$, giving lattice parameters of $a_{fcc} = b_{fcc} = 4.20$ Å, $c_{fcc} = 3.95$ Å, $\alpha_{fcc} = \beta_{fcc} = 90.1°$, $\gamma_{fcc} = 92.7°$. This pseudo-cubic representation provides a straightforward understanding of the crystal shape, thereby facilitating systematic exploration of its crystal orientations. © 2026 The Author(s). Published on behalf of The Japan Society of Applied Physics by IOP Publishing Ltd

Supplementary material for this article is available online

Recently, β-Ga_2O_3 has attracted increasing attention as a promising semiconductor for ultraviolet optoelectronics and power electronics,[1,2] owing to its large bandgap ($\geqslant$4.43 eV)[3] and the availability of scalable, melt-grown single crystals.[4] In particular, the availability of low-defect native substrates[4] provides a reproducible platform for the optimization of homoepitaxy[5] and device processing,[6] thereby enabling rapid device demonstration.[1,2] However, establishing clear guidelines for substrate orientation selection and the associated process design remains challenging owing to its low-symmetry monoclinic structure,[7] in contrast to conventional semiconductors with high-symmetry crystal structures (e.g. diamond, zinc blende, and wurtzite structures).

β-Ga_2O_3 crystallizes in the monoclinic system (space group C2/m) and has lattice parameters of $a = 12.214$ Å, $b = 3.0371$ Å, $c = 5.7981$ Å, $\alpha = 90°$, $\beta = 103.83°$, and $\gamma = 90°$.[7] This monoclinic structure, unique to β-Ga_2O_3 and θ-Al_2O_3,[8] hampers an intuitive understanding of crystal orientations. For example, the planes that are exactly and nearly perpendicular to (100) are {010} and $\{\bar{1}12\}/\{\bar{1}02\}$, respectively; however, such orientation relationships are not readily apparent from the monoclinic unit cell. Therefore, an alternative and more straightforward representation is required to facilitate understanding of this complex crystal structure.

A useful way to obtain a more intuitive picture of the low-symmetry monoclinic structure of β-Ga_2O_3 is to view it from the oxygen sublattice. The oxygen sublattice governs the crystal framework of β-Ga_2O_3 because oxygen ions have larger ionic radii (1.36 and 1.38 Å for threefold and fourfold coordination, respectively) than gallium ions (0.47 and 0.62 Å for fourfold and sixfold coordination, respectively).[9] The oxygen ions in β-Ga_2O_3 are known to form a cubic close-packed (ccp) arrangement and can be regarded as a slightly distorted face-centered cubic (fcc) structure.[7,10]

This oxygen-framework-based viewpoint has often been employed to facilitate the understanding of various phenomena in β-Ga_2O_3 and other Ga_2O_3 polymorphs. For example, slip systems in β-Ga_2O_3 have been discussed in relation to oxygen ccp planes, accompanied by experimental observations of dislocation formation.[11,12] In addition, the crystal structures of Ga_2O_3 polymorphs (α, β, γ, ε, and κ) can be broadly understood in terms of whether the oxygen sublattice adopts hexagonal close packing or ccp and how Ga-site occupancy is arranged within the framework,[13] which also helps rationalize structural changes during phase transitions (e.g. $\alpha\rightarrow\beta$, $\gamma\rightarrow\beta$, $\varepsilon\rightarrow\beta$, and $\kappa\rightarrow\beta$).[14–17] Notably, because β- and γ-Ga_2O_3 share the same ccp oxygen framework, radiation-induced $\beta\rightarrow\gamma$ transformations can preserve the oxygen sublattice, thereby accounting for the high radiation tolerance.[18] Furthermore, the fcc-based framework provides a convenient basis for describing heteroepitaxial orientation relationships between β-Ga_2O_3 and other cubic materials.[19,20]

Despite these demonstrated utilities, detailed and consolidated information on the oxygen-sublattice-based pseudo-cubic framework of β-Ga_2O_3—such as the averaged fcc lattice parameters and the correspondence between primary fcc planes and monoclinic β-Ga_2O_3 planes—has not yet been summarized in a single, systematic form. Therefore, in this Brief Note, we provide a unified and readily accessible summary of this pseudo-cubic representation.

Here, we first define the averaged fcc reference unit cell for the oxygen sublattice. The averaged fcc structure can be defined by lattice vectors: $\boldsymbol{a}_{\mathbf{fcc}} = \boldsymbol{b} + 1/2\ \boldsymbol{c}$, $\boldsymbol{b}_{\mathbf{fcc}} = -\boldsymbol{b} + 1/2\ \boldsymbol{c}$, and $\boldsymbol{c}_{\mathbf{fcc}} = 1/3\ \boldsymbol{a} + 1/6\ \boldsymbol{c}$, where $\boldsymbol{a}$, $\boldsymbol{b}$, and $\boldsymbol{c}$ are lattice vectors of monoclinic β-Ga_2O_3, as shown in Fig. 1. Here, $\boldsymbol{a}_{\mathbf{fcc}}$, $\boldsymbol{b}_{\mathbf{fcc}}$, and $\boldsymbol{c}_{\mathbf{fcc}}$ are not fcc primitive lattice vectors but rather define a non-primitive fcc-based reference unit cell for the averaged oxygen sublattice (see Fig. 1). Note that the assignment of the directions of $\boldsymbol{a}_{\mathbf{fcc}}$, $\boldsymbol{b}_{\mathbf{fcc}}$, and $\boldsymbol{c}_{\mathbf{fcc}}$ is not unique and may be permuted. In the present definition, $\boldsymbol{a}_{\mathbf{fcc}}$ and $\boldsymbol{b}_{\mathbf{fcc}}$ are crystallographically equivalent, reflecting the symmetric equivalence of the $\boldsymbol{b}$ and $-\boldsymbol{b}$ directions in the monoclinic lattice.

From the fcc lattice vectors, the corresponding lattice parameters are calculated to be $a_{fcc} = b_{fcc} = 4.20$ Å, $c_{fcc} = 3.95$ Å, $\alpha_{fcc} = \beta_{fcc} = 90.1°$, and $\gamma_{fcc} = 92.7°$. The deviation from an ideal cubic lattice is relatively small,

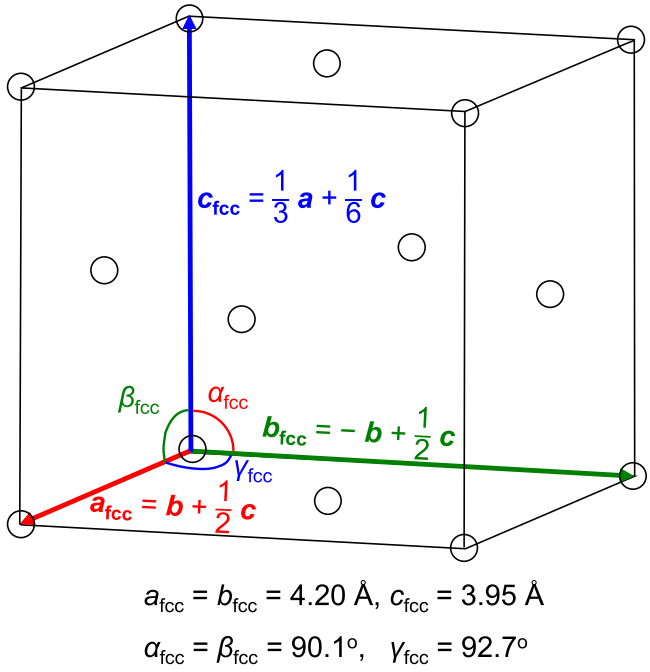

Fig. 1. Averaged pseudo-cubic unit cell of the distorted face-centered cubic (fcc) oxygen sublattice in β-Ga_2O_3. The unit cell is defined by the lattice vectors $\boldsymbol{a}_{fcc}$, $\boldsymbol{b}_{fcc}$, and $\boldsymbol{c}_{fcc}$, giving lattice parameters of a_{fcc}, b_{fcc}, c_{fcc}, α_{fcc}, β_{fcc}, and γ_{fcc}. Oxygen atoms are placed at the fcc sites and are shown in the unit cell as open circles.

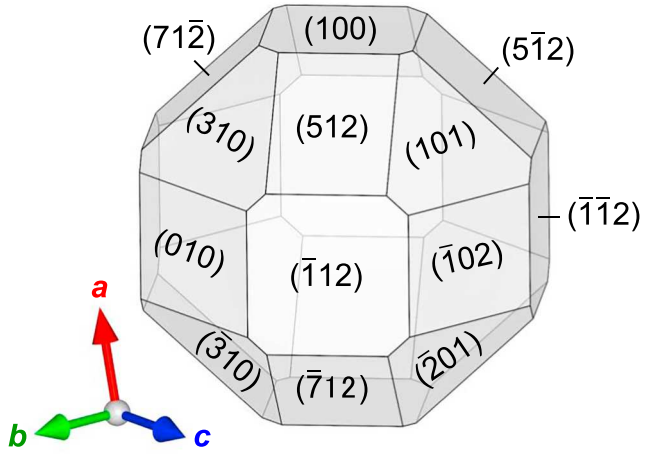

Fig. 2. Crystal shape faceted with the representative oxygen sublattice planes of β-Ga_2O_3. The Miller indices of the hidden $(\bar{h}\bar{k}\bar{l})$ facets can be identified because they are crystallographically equivalent to their opposite (hkl) facets that are already labeled.

justifying the use of pseudo-cubic approximation, which greatly facilitates the understanding of the crystal structure.

In the cubic fcc oxygen structure, the principal crystallographic planes are $\{100\}_{fcc}$ (6 planes), $\{110\}_{fcc}$ (12 planes), and $\{111\}_{fcc}$ (8 planes). All of these planes have corresponding planes in monoclinic β-Ga_2O_3, as summarized in Table I. Note that (hkl), $(\bar{h}\bar{k}\bar{l})$, $(h\bar{k}l)$, and $(\bar{h}k\bar{l})$ planes are crystallographically equivalent. Figure 2 shows the crystal shape constructed using all the planes listed in Table I. This three-dimensional shape was visualized using the crystallographic visualization software VESTA,[21,22] assuming that each crystal facet is located at an equal distance from the origin. We also prepared a printable papercraft template to build a physical model of this crystal shape, enabling hands-on inspection of its three-dimensional geometry (see the supplementary file).

Table I presents the primary crystallographic planes of the oxygen fcc sublattice. The {100} and $\{\bar{1}12\}$ planes are among the most fundamental, as they correspond to the six $\{100\}_{fcc}$ faces of the pseudo-cubic structure. The $\{\bar{2}01\}$, {101}, and {310} planes exhibit oxygen close-packed configurations corresponding to the $\{111\}_{fcc}$ planes, whereas the {010}, $\{\bar{1}02\}$, {512}, and $\{\bar{7}12\}$ planes correspond to the low-index $\{110\}_{fcc}$ planes. Several of these planes have not yet been selected as substrate orientations; therefore, their investigation may be worthwhile for exploring new substrate orientations. Note that the (001) plane—the most commonly used substrate orientation for vertical power devices—is not included in Table I; instead, the $(\bar{1}02)$ plane, which is crystallographically close to (001),[23–25] is included. Similarly, the (011) plane—another substrate orientation that has recently attracted attention for vertical power devices[26–29]—is also excluded from the Table I, whereas the $(\bar{1}12)$ plane, which is close to (011) is included.

Figure 2 clearly illustrates the orientation relationships of these planes, particularly the orthogonal and nearly orthogonal relationships resulting from the pseudo-cubic approximation. For example, the (100) plane is perpendicular to the {010} and almost perpendicular to the $\{\bar{1}12\}$ and $\{\bar{1}02\}$ planes with interplanar angles of 89.9° and 89.9°, respectively; the (010) plane is perpendicular to the {100}, $\{\bar{1}02\}$, {101}, and $\{\bar{2}01\}$ planes; the $(\bar{1}02)$ plane is perpendicular to {010} and almost perpendicular to {100} and {310} with interplanar angles of 89.9° and 89.9°, respectively; and the $(\bar{2}01)$ plane is perpendicular to {010} and nearly perpendicular to {512} with an interplanar angle of 91.7°. This information is particularly useful when considering combinations of substrate orientations and sidewall planes formed by etching processes. In plasma-free gas etching, the (100) surface becomes exceptionally flat as it exhibits the minimum surface energy density.[30] Therefore, trenches and fins with (100)-faceted vertical and near-vertical sidewalls should be fabricated using gas etching by employing substrates oriented along {010} and $\{\bar{1}12\}/\{\bar{1}02\}$, respectively. This approach has been experimentally verified with (010) and $(\bar{1}02)$ substrates.[24,31–35]

Furthermore, the correspondence between the fcc and monoclinic planes summarized in Table I allows direct estimation of epitaxial relationships between cubic crystals and β-Ga_2O_3. Since β-Ga_2O_3 is a unipolar n-type semiconductor, the realization of p–n junctions relies on the

Table I. Correspondence between crystallographic planes of the slightly distorted face-centered cubic (fcc) oxygen sublattice and monoclinic β-Ga_2O_3.

fcc oxygen sublattice planes	Corresponding planes in monoclinic β-Ga_2O_3
$\{100\}_{fcc}$	(100), $(\bar{1}00)$, $(\bar{1}12)$, $(1\bar{1}\bar{2})$, $(\bar{1}\,\bar{1}2)$, $(11\bar{2})$
$\{110\}_{fcc}$	(010), $(0\bar{1}0)$, $(\bar{1}02)$, $(10\bar{2})$, (512), $(\bar{5}\,\bar{1}\,\bar{2})$, $(5\bar{1}2)$, $(\bar{5}1\bar{2})$, $(\bar{7}12)$, $(7\bar{1}\bar{2})$, $(\bar{7}\,\bar{1}2)$, $(71\bar{2})$
$\{111\}_{fcc}$ (Close packing planes)	$(\bar{2}01)$, $(20\bar{1})$, (101), $(\bar{1}0\bar{1})$, (310), $(\bar{3}\,\bar{1}0)$, $(3\bar{1}0)$, $(\bar{3}10)$

heteroepitaxial growth of p-type oxides, particularly rock-salt-structured NiO ($a = 4.1684$ Å).[36,37] Therefore, determining the epitaxial relationships between cubic NiO and monoclinic β-Ga_2O_3 is essential for understanding p–n heterojunctions, and such relationships can be readily estimated using Table I. For example, (100)-oriented NiO should be obtained on {100} and {$\bar{1}$12} β-Ga_2O_3 substrates. The validity of this correspondence has been experimentally demonstrated in several studies. To date, (100)-, (110)-, (110)- and (111)-oriented NiO films have been epitaxially grown on (100), (010), ($\bar{1}$02), and ($\bar{2}$01) β-Ga_2O_3 substrates, respectively.[25,38,39] Similar oxygen-sublattice-aligned epitaxy has also been reported for other cubic oxides grown on β-Ga_2O_3 substrates, further supporting the validity of this approach. For p-type materials other than NiO, reported examples include (100) and (110) $NiGa_2O_4$ (spinel structure, $a = 8.258\,95$ Å)[40] on (100) and (010) β-Ga_2O_3, respectively;[41] (111) Cr_2MnO_4 (spinel structure, $a = 8.41$ Å)[42] on ($\bar{2}$01) β-Ga_2O_3;[43] and (1$\bar{1}$0) $LiGa_5O_8$ (spinel structure, $a = 8.203$ Å)[44] on (010) β-Ga_2O_3.[45] For dielectric materials, reported examples include (110) γ-Al_2O_3 (defective spinel structure, $a = 7.911$ Å)[46] on (010) β-Ga_2O_3;[47] and (110) and (100) γ-$(Al_xGa_{1-x})_2O_3$ (defective spinel structure) on (010) and (100) β-Ga_2O_3, respectively.[48,49]

In summary, we systematically investigated a pseudo-cubic description of monoclinic β-Ga_2O_3 based on its distorted fcc oxygen sublattice. By defining an averaged fcc unit cell and establishing the correspondence between fcc and monoclinic planes, the complex orientation relationships of β-Ga_2O_3 can be understood in an intuitive and straightforward manner. This approach identifies the primary planes constituting the oxygen sublattice, clarifies the orthogonal relationships among these planes, enables reasonable selection of substrate orientations suitable for vertical etching, and allows estimation of epitaxial relationships with cubic oxides such as NiO. The pseudo-cubic representation therefore provides a practical crystallographic basis for β-Ga_2O_3 and is useful for screening unexplored substrate orientations.

Acknowledgments This work was financially supported by a Grant-in-Aid for Scientific Research (B) from the Japan Society for the Promotion of Science (JSPS), MEXT, Japan (No. JP24K01368).

ORCID iDs Takayoshi Oshima https://orcid.org/0000-0001-8550-9735

1) S. J. Pearton, F. Ren, A. Y. Polyakov, A. Haque, M. Labed, and Y. S. Rim, Appl. Phys. Rev. **12**, 031336 (2025).
2) K. Sasaki, Appl. Phys. Express **17**, 090101 (2024).
3) T. Onuma, S. Saito, K. Sasaki, T. Masui, T. Yamaguchi, T. Honda, and M. Higashiwaki, Jpn. J. Appl. Phys. **54**, 112601 (2015).
4) X. Wang, X. Chang, P. Wang, X. Yang, and L. Yuan, Cryst. Res. Technol. **60**, 2400255 (2025).
5) I. Rahaman, H. D. Ellis, C. Chang, D. H. Mudiyanselage, M. Xu, B. Da, H. Fu, Y. Zhao, and K. Fu, Materials **17**, 4261 (2024).
6) S. Sun, C. Wang, S. Alghamdi, H. Zhou, Y. Hao, and J. Zhang, Adv. Electron. Mater. **11**, 2300844 (2025).
7) J. Åhman, G. Svensson, and J. Albertsson, Acta Crystallogr. C **52**, 1336 (1996).
8) J. A. Kohn, G. Katz, and J. D. Broder, Am. Mineral. **42**, 398 (1957).
9) R. D. Shannon, Acta Crystallogr. A **32**, 751 (1976).
10) S. Geller, J. Chem. Phys. **33**, 676 (1960).
11) H. Yamaguchi, A. Kuramata, and T. Masui, Superlattices Microstruct. **99**, 99 (2016).
12) H. Yamaguchi and A. Kuramata, J. Appl. Crystallogr. **51**, 1372 (2018).
13) H. Y. Playford, A. C. Hannon, E. R. Barney, and R. I. Walton, Chem.-Eur. J. **19**, 2803 (2013).
14) S.-C. Zhu, S.-H. Guan, and Z.-P. Liu, Phys. Chem. Chem. Phys. **18**, 18563 (2016).
15) C. Wouters, M. Nofal, P. Mazzolini, J. Zhang, T. Remmele, A. Kwasniewski, O. Bierwagen, and M. Albrecht, APL Mater. **12**, 011110 (2024).
16) Z. Zolnai, P. Petrik, A. Németh, J. Volk, M. Bosi, L. Seravalli, and R. Fornari, Appl. Surf. Sci. **636**, 157869 (2023).
17) I. Cora, Z. Fogarassy, R. Fornari, M. Bosi, A. Rečnik, and B. Pécz, Acta Mater. **183**, 216 (2020).
18) R. He, J. Zhao, J. Byggmästar, H. He, and F. Djurabekova, Phys. Rev. Mater. **8**, 084601 (2024).
19) T. Hadamek, A. B. Posadas, F. Al-Quaiti, D. J. Smith, M. R. McCartney, and A. A. Demkov, AIP Adv. **11**, 045209 (2021).
20) T. Hadamek, A. B. Posadas, F. Al-Quaiti, D. J. Smith, M. R. McCartney, E. Dombrowski, and A. A. Demkov, J. Appl. Phys. **131**, 145702 (2022).
21) K. Momma and F. Izumi, J. Appl. Crystallogr. **41**, 653 (2008).
22) K. Momma and F. Izumi, J. Appl. Crystallogr. **44**, 1272 (2011).
23) Y. Oshima and T. Oshima, Semicond. Sci. Technol. **38**, 105003 (2023).
24) T. Oshima and Y. Oshima, Appl. Phys. Lett. **124**, 042110 (2024).
25) T. Oshima and S. Nakagomi, Jpn. J. Appl. Phys. **62**, 128001 (2023).
26) K. Goto, H. Murakami, A. Kuramata, S. Yamakoshi, M. Higashiwaki, and Y. Kumagai, Appl. Phys. Lett. **120**, 102102 (2022).
27) Y. Oshima and T. Oshima, Sci. Technol. Adv. Mater. **26**, 2585551 (2025).
28) T. Oshima and Y. Oshima, Jpn. J. Appl. Phys. **64**, 018003 (2025).
29) D. Wakimoto, C.-H. Lin, K. Ema, Y. Ueda, H. Miyamoto, K. Sasaki, and A. Kuramata, Appl. Phys. Express **18**, 106502 (2025).
30) T. Oshima and Y. Oshima, Appl. Phys. Lett. **122**, 162102 (2023).
31) T. Oshima and Y. Oshima, Appl. Phys. Express **16**, 066501 (2023).
32) T. Oshima, R. Togashi, and Y. Oshima, Sci. Technol. Adv. Mater. **25**, 2378683 (2024).
33) N. K. Kalarickal et al., Appl. Phys. Lett. **119**, 123503 (2021).
34) S. A. Khan, A. Ibreljic, and A. F. M. A. U. Bhuiyan, Appl. Phys. Lett. **127**, 102105 (2025).
35) N. Das, F. Alema, W. Brand, A. Katta, A. Gilankar, A. Osinsky, and N. K. Kalarickal, J. Appl. Phys. **138**, 065703 (2025).
36) R. W. Cairns and E. Ott, J. Am. Chem. Soc. **55**, 527 (1933).
37) Y. Kokubun, S. Kubo, and S. Nakagomi, Appl. Phys. Express **9**, 091101 (2016).
38) S. Nakagomi, T. Yasuda, and Y. Kokubun, Phys. Status Solidi **257**, 1900669 (2020).
39) G. Yasui, H. Miyake, K. Shimazoe, and H. Nishinaka, Phys. Status Solidi **262**, 2400442 (2025).
40) A. Sharma, M. Varshney, Y. Kumar, A. Vij, R. K. Sharma, and H.-J. Shin, J. Electron. Mater. **51**, 4139 (2022).
41) K. Egbo et al., arXiv:2512.20841 (2025).
42) R. N. Bhowmik, R. Ranganathan, and R. Nagarajan, Phys. Rev. B **73**, 144413 (2006).
43) K. Zhang, V. G. T. Vangipuram, C. Chae, J. Hwang, and H. Zhao, Appl. Phys. Lett. **124**, 122106 (2024).
44) S. M. Sadman and W. R. L. Lambrecht, Phys. Rev. B **112**, 1 (2025).
45) B. Akintunde et al., J. Appl. Phys. **138**, 215301 (2025).
46) R.-S. Zhou and R. L. Snyder, Acta Crystallogr. B **47**, 617 (1991).
47) M. Hattori et al., Jpn. J. Appl. Phys. **55**, 1202B6 (2016).
48) R. Wakabayashi, T. Oshima, M. Hattori, K. Sasaki, T. Masui, A. Kuramata, S. Yamakoshi, K. Yoshimatsu, and A. Ohtomo, J. Cryst. Growth **424**, 77 (2015).
49) R. Wakabayashi, K. Yoshimatsu, M. Hattori, J.-S. Lee, O. Sakata, and A. Ohtomo, Cryst. Growth Des. **21**, 2844 (2021).